IET Power Electronics

Research Article

IET Journals
The Institution of Engineering and Technology

Output voltage tracking controller embedding auto-tuning algorithm for DC/DC boost converters

ISSN 1755-4535
Received on 21st September 2018
Revised 6th September 2019
Accepted on 17th September 2019
E-First on 21st October 2019
doi: 10.1049/iet-pel.2018.6021
www.ietdl.org

Kyunghwan Choi[1], Yonghun Kim[2], Kyung-Soo Kim[1], Seok-Kyoon Kim[3] ✉

[1]*Department of Mechanical Engineering, Korea Advanced Institute of Science and Technology, Daejeon 34141, Republic of Korea*
[2]*Eco-friendly Smart Vehicle Research Center, Korea Advanced Institute of Science and Technology, Daejeon 34141, Republic of Korea*
[3]*Department of Creative Convergence Engineering, Hanbat National University, Daejeon 34158, Republic of Korea*
✉ *E-mail: lotus45kr@gmail.com*

Abstract: This study suggests a non-linear output voltage tracking controller for DC/DC boost converters in the form of a classical cascade control structure. Non-linearities in the converter dynamics as well as parameter uncertainties and load variations are considered. The first contribution of this study is the design of an auto-tuner, which automatically adjusts the control gain according to the output voltage error to enhance transient performance. The second contribution involves proving that the closed-loop system ensures the performance recovery without any steady-state errors in the presence of parameter and load variations. The effectiveness of the proposed algorithm was verified through experimental investigations using a 5 kW prototype DC/DC boost converter.

1 Introduction

DC/DC boost converters have been widely used in industrial applications such as solar/wind power systems, electrical vehicles, and various home appliances [1–6], owing to their advantages such as satisfactory regulation performance for the output voltage and inductor current, and power factor correction.

The cascade output voltage regulator has been regarded as a conventional control system for DC/DC boost converters, where the outer voltage control loop provides a reference signal to the inner current control loop [7]. The cascade control regulator is usually designed using proportional–integral (PI) controllers to provide each loop with two degrees of freedom. The Bode plot and Nyquist techniques can be utilised to adjust the resultant closed-loop performance of the cascade loops through gain tuning in the frequency domain [7, 8]. A feedback-linearisation (FL) technique was suggested, which combines the PI control scheme with the feedforward compensation of parameter-dependent terms in the converter, where the PI gains for tuning the cut-off frequency of the closed-loop system are dependent on the converter parameters [7]. Hence, the accuracy of the parameter information has critical effects on the closed-loop performance. The parameter dependency of the FL technique can be reduced by incorporating the gain scheduling scheme [9, 10].

It has been shown that the implementation of advanced techniques can improve the closed-loop performance over that of the conventional techniques. Adaptive [11, 12], robust [13], and sliding mode [14, 15] control schemes have been proposed to cope with the parameter uncertainties and load variations, and predictive [16] and model predictive [17–20] controllers have been investigated to improve the tracking performance of the output voltage control. On the other hand, achieving fast transient responses is also an important requirement in industrial applications, which is directly related to the product quality. An intuitive way to achieve fast transient responses is to increase the closed-loop cut-off frequency by increasing the control gains, but it also involves increasing the sensitivity of the control system. A deadbeat controller [21] can be used to achieve the minimum rise and settling times for the voltage control. However, the deadbeat controller is highly sensitive to system uncertainties such as parameter and load variations. To the best of our knowledge, no studies have been conducted to resolve the trade-off between improving the transient response and increasing the sensitivity of the control system while maintaining robustness to system uncertainties.

In this study, an auto-tuning algorithm for the closed-loop cut-off frequency of the output voltage control is investigated as a means of resolving the trade-off discussed above. This scheme differs from previous studies that use a fixed cut-off frequency. The contributions of this study are listed as follows:

- An auto-tuner, which increases the control gain in a transient state and returns the control gain to its initial value in a steady state, is designed to enhance transient performance while maintaining the sensitivity of the control system in steady states.
- Non-linear disturbance observers (DOBs) are utilised to estimate and compensate the disturbances arising from parameter and load uncertainties.
- It is proved that a proportional-type output voltage tracking controller embedding the auto-tuner and DOBs ensures the exponential convergence and the performance recovery property without any steady-state errors.

The effectiveness of the proposed controller is confirmed based on the experimental data obtained using a 5 kW prototype DC/DC boost converter control system.

2 Dynamics of DC/DC boost converters

The section provides a brief introduction to the dynamical equations for describing the non-linear behaviour of the DC/DC boost converters depicted in Fig. 1. By applying the averaging technique to this converter topology, it holds that [7]

$$L\frac{\mathrm{d}i_L(t)}{\mathrm{d}t} = v_{\mathrm{in}}(t) - (1-u(t))v_{\mathrm{dc}}(t), \tag{1}$$

$$C\frac{\mathrm{d}v_{\mathrm{dc}}(t)}{\mathrm{d}t} = (1-u(t))i_L(t) - i_{\mathrm{Load}}(t), \tag{2}$$

where $i_L(t)$ and $v_{\mathrm{dc}}(t)$ denote the current passing through the inductor L and the voltage across the output capacitor C, respectively, and $u(t)$ represents the duty ratio for the switching device, which is feasible on the set of [0,1]. The input DC source voltage and load current are given as $v_{\mathrm{in}}(t)$ and $i_{\mathrm{Load}}(t)$, respectively.

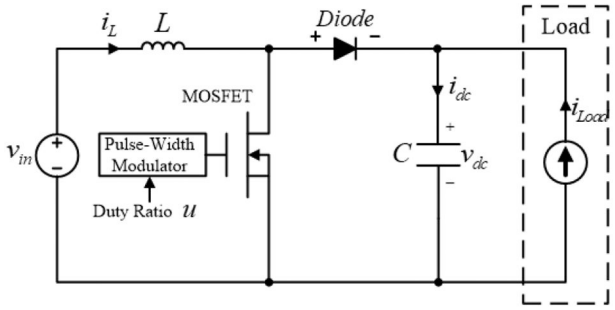

Fig. 1 *Topology of a DC/DC boost converter*

In this study, $i_L(t)$ and $v_{\rm dc}(t)$ are considered as the available state-variables with the control input of $u(t)$.

For the implementation of a control system, it is reasonable to assume that

- The values of the inductor and capacitor are difficult to determine exactly, except for their nominal values L_0 and C_0.
- The exact value of the DC source voltage $v_{\rm in}(t)$ is also difficult to determine, possibly owing to a resistive drop of the source, except for its initial voltage value $v_{\rm in,0} = v_{\rm in}(0)$.
- The time-varying signal $i_{\rm Load}(t)$ represents a generic load, which includes both linear and non-linear loads.

The following section devises a control law for the reference inductor current of $i_{L,\rm ref}(t)$ and the duty ratio of $u(t)$ in combination with an auto-tuner and DOBs.

3 Output voltage controller development

For any given reference output voltage $v_{\rm dc,ref}(t)$, the desired closed-loop output voltage dynamics of $v^*_{\rm dc}(t)$ is described by

$$\dot{v}^*_{\rm dc}(t) = \omega_{vc}(v_{\rm dc,ref}(t) - v^*_{\rm dc}(t)),$$

with a cut-off frequency $\omega_{\rm vc}$, whose tracking performance can be enhanced by replacing $\omega_{\rm vc}$ with $\hat{\omega}_{\rm vc}(t)$ as

$$\dot{v}^*_{\rm dc}(t) = \hat{\omega}_{vc}(t)(v_{\rm dc,ref}(t) - v^*_{\rm dc}(t)), \tag{3}$$

where $\hat{\omega}_{\rm vc}(t)$ denotes an adjustable cut-off frequency to be designed later, which is considered as the target output voltage dynamics.

The control objective involves forcing the output voltage dynamics to behave as the target dynamics of (3) by designing the control input of $u(t)$. To this end, Section 3.1 presents a derivation of the control law, including an auto-tuner and DOBs. The behaviour of the closed-loop system is analysed in Section 3.2.

3.1 Controller design

The converter dynamics (1)–(2) can be rewritten as

$$L_0\frac{{\rm d}i_L(t)}{{\rm d}t} = v_{\rm in,0} - (1-u(t))v_{\rm dc}(t) + d_{L,0}(t), \tag{4}$$

$$C_0\frac{{\rm d}v_{\rm dc}(t)}{{\rm d}t} = (1-u(t))i_L(t) + d_v(t), \tag{5}$$

with an initial input voltage value $v_{\rm in,0}$ and the nominal parameters L_0 and C_0, where $d_{L,0}(t)$ and $d_v(t)$ denote the lumped disturbances representing the model-plant mismatches and load variations, respectively, which are to be estimated and compensated by the DOBs. Section 3.1.1 designs the outer loop with an auto-tuner by considering the reference inductor current $i_{L,\rm ref}(t)$ as a design variable. The control input of $u(t)$ for stabilising the inductor current error dynamics is derived in Section 3.1.2.

3.1.1 Outer loop: The outer-loop design begins by expressing the output voltage dynamics of (5) with the reference inductor current $i_{L,\rm ref}(t)$ and the inductor current error defined by $\tilde{i}_L(t) := i_{L,\rm ref}(t) - i_L(t)$ as

$$\begin{aligned} C_0\dot{v}_{\rm dc}(t) = {} & (1-u(t))i_{L,\rm ref}(t) - (1-u(t))\tilde{i}_L(t) \\ & + d_v(t)\,. \end{aligned} \tag{6}$$

The reference inductor current $i_{L,\rm ref}(t)$ is given by

$$i_{L,\rm ref}(t) = \frac{1}{1-u(t)}(C_0\hat{\omega}_{vc}(t)\tilde{v}_{\rm dc}(t) - \hat{d}_v(t)), \tag{7}$$

where the output voltage tracking error is defined by $\tilde{v}_{\rm dc}(t) := v_{\rm dc,ref}(t) - v_{\rm dc}(t)$ with its reference of $v_{\rm dc,ref}(t)$, and $\hat{d}_v(t)$ and $\hat{\omega}_{vc}(t)$ denote the estimated disturbance and adjustable control gain, respectively. The auto-tuner for $\hat{\omega}_{vc}(t)$ is proposed as

$$\dot{\hat{\omega}}_{vc}(t) = \gamma_{\rm at}(\tilde{v}^2_{\rm dc}(t) + \rho_{\rm at}\tilde{\omega}_{vc}(t)), \tag{8}$$

with $\tilde{\omega}_{vc}(t) := \omega_{vc} - \hat{\omega}_{vc}(t)$, $\hat{\omega}_{vc}(0) = \omega_{vc}$, and the design parameters $\gamma_{at} > 0$ and $\rho_{at} > 0$. The term $\gamma_{at}\tilde{v}^2_{dc}(t)$ is used to increase the control gain in a transient state in which the output voltage tracking error is non-zero. The term $\rho_{\rm at}\tilde{\omega}_{vc}(t)$ functions as a damping component that returns the increased control gain to its initial value $\hat{\omega}_{vc}(0)$ after the transient state is over. The estimated disturbance $\hat{d}_v(t)$ originates from

$$\dot{z}_v(t) = -l_v z_v(t) - l_v^2 C_0 v_{\rm dc}(t) - l_v(1-u(t))i_L(t), \tag{9}$$

$$\hat{d}_v(t) = z_v(t) + l_v C_0 v_{\rm dc}(t), \tag{10}$$

with the design parameter $l_v > 0$. Then, the combination of (6)–(8) provides the closed-loop error dynamics as

$$\begin{aligned} \dot{\tilde{v}}_{\rm dc}(t) = {} & -\omega_{vc}\tilde{v}_{\rm dc}(t) + \frac{(1-u(t))}{C_0}\tilde{i}_L(t) \\ & + \tilde{\omega}_{vc}(t)\tilde{v}_{\rm dc}(t) - \frac{1}{C_0}\tilde{d}_v(t) + \dot{v}_{\rm dc,ref}(t), \end{aligned} \tag{11}$$

$$\dot{\tilde{\omega}}_{vc}(t) = -\gamma_{\rm at}(\tilde{v}^2_{\rm dc}(t) + \rho_{\rm at}\tilde{\omega}_{vc}(t)), \tag{12}$$

which is utilised in the closed-loop analysis.

3.1.2 Inner loop: The inductor current dynamics of (4) can be written using the inductor current error $\tilde{i}_L(t)$ as

$$L_0\dot{\tilde{i}}_L(t) = -v_{\rm in,0} + (1-u(t))v_{\rm dc}(t) + d_L(t), \tag{13}$$

where $d_L(t) := L_0\dfrac{di_{L,\rm ref}(t)}{{\rm d}t} - d_{L,0}(t)$, which can be stabilised by the proposed control input

$$u(t) = 1 + \frac{1}{v_{\rm dc}(t)}\left(L_0\omega_{cc}\tilde{i}_L(t) - v_{\rm in,0} + \hat{d}_L(t)\right), \tag{14}$$

with the design parameter $\omega_{cc} > 0$, where the estimated disturbance $\hat{d}_L(t)$ originates from

$$\begin{aligned} \dot{z}_L(t) = {} & -l_L z_L(t) - l_L^2 L_0\tilde{i}_L(t) \\ & + l_L(v_{\rm in,0} - (1-u(t))v_{\rm dc}(t)), \end{aligned} \tag{15}$$

$$\hat{d}_L(t) = z_L(t) + l_L L_0\tilde{i}_L(t), \tag{16}$$

with the design parameter $l_v > 0$. Then, the combination of (13)–(14) provides the closed-loop dynamics as

$$\dot{\tilde{i}}_L(t) = -\omega_{cc}\tilde{i}_L(t) + \frac{1}{L_0}\tilde{d}_L(t), \tag{17}$$

which is used for the closed-loop analysis.

3.2 Closed-loop analysis

This section presents and proves useful closed-loop properties of the proposed controller. First, Theorem 1 provides the exponential convergence property to the reference output voltage $v_{\mathrm{dc,ref}}(t)$.

Theorem 1: The proposed control law of (14) with the reference inductor current of (7), DOBs of (9), (10), (15), and (16), and the auto-tuner of (8) guarantees the exponential convergence property, i.e.

$$\lim_{t\to\infty} v_{\mathrm{dc}}(t) = v_{\mathrm{dc,ref}}(t) \tag{18}$$

as $\dot{v}_{\mathrm{dc,ref}}(t), \dot{d}_v(t)$, and $\dot{d}_L(t)$ tend exponentially towards zero.

Proof: It follows from the combination of (9), (10), (15), and (16) that

$$\begin{aligned}\dot{\hat{d}}_v - l_v C_0 \dot{v}_{\mathrm{dc}} =& -l_v(\hat{d}_v - l_v C_0 v_{\mathrm{dc}}) - l_v^2 C_0 v_{\mathrm{dc}} \\ & - l_v(1-u)i_L,\end{aligned}$$

$$\begin{aligned}\dot{\hat{d}}_L - l_L L_0 \dot{\tilde{i}}_L =& -l_L(\hat{d}_L - l_L L_0 \tilde{i}_L) - l_L^2 L_0 \tilde{i}_L \\ & + l_L(v_{\mathrm{in},0} - (1-u)v_{\mathrm{dc}}),\end{aligned}$$

which can be rearranged using (6) and (13) as

$$\dot{\tilde{d}}_k = -l_k\tilde{d}_k + \dot{d}_k, \quad k = v, L, \tag{19}$$

with $\tilde{d}_k := d_k - \hat{d}_k$, $k = v, L$. Then, the positive definite function given by

$$\begin{aligned}V :=& \frac{1}{2}\tilde{v}_{\mathrm{dc}}^2 + \frac{\kappa}{2}\tilde{i}_L^2 + \frac{1}{2\gamma_{\mathrm{at}}}\tilde{\omega}_{vc}^2 + \sum_{k=v,L}\frac{\kappa_k}{2}\tilde{d}_k^2, \\ & \kappa > 0, \kappa_k > 0,\end{aligned} \tag{20}$$

yields its time derivative along the trajectories of (11), (12), (17), and (19) as follows:

$$\begin{aligned}\dot{V} &= \tilde{v}_{\mathrm{dc}}\dot{\tilde{v}}_{\mathrm{dc}} + \kappa\tilde{i}_L\dot{\tilde{i}}_L + \frac{1}{\gamma_{\mathrm{at}}}\tilde{\omega}_{vc}\dot{\tilde{\omega}}_{vc} + \sum_{k=v,L}\kappa_k\tilde{d}_k\dot{\tilde{d}}_k \\ &= \tilde{v}_{\mathrm{dc}}\Big(-\omega_{vc}\tilde{v}_{\mathrm{dc}} + \frac{(1-u)}{C_0}\tilde{i}_L + \tilde{\omega}_{vc}\tilde{v}_{\mathrm{dc}} - \frac{1}{C_0}\tilde{d}_v \\ &\quad + \dot{v}_{\mathrm{dc,ref}}\Big) + \kappa\tilde{i}_L\Big(-\omega_{cc}\tilde{i}_L + \frac{1}{L_0}\tilde{d}_L\Big) \\ &\quad - \tilde{\omega}_{vc}(\tilde{v}_{\mathrm{dc}}^2 + \rho_{\mathrm{at}}\tilde{\omega}_{vc}) \\ &\quad - \sum_{k=v,L}\kappa_k l_k\tilde{d}_k^2 + \sum_{k=v,L}\kappa_k\tilde{d}_k\dot{d}_k.\end{aligned}$$

An upper bound of $\dot{V}$ is derived using the Young's inequality $xy \le \frac{\epsilon}{2}x^2 + \frac{1}{2\epsilon}y^2$ for $\forall\epsilon > 0$ as

$$\begin{aligned}\dot{V} \le& -\frac{\omega_{vc}}{3}\tilde{v}_{\mathrm{dc}}^2 - \Big(\kappa\omega_{cc} - \frac{3}{4\omega_{vc}C_0^2} - \frac{1}{2}\Big)\tilde{i}_L^2 - \rho_{\mathrm{at}}\tilde{\omega}_{vc}^2 \\ & + \tilde{v}_{\mathrm{dc}}\dot{v}_{\mathrm{dc,ref}} - \Big(\kappa_v l_v - \frac{3}{4\omega_{vc}C_0^2}\Big)\tilde{d}_v^2 \\ & - \Big(\kappa_L l_L - \frac{\kappa^2}{2L_0^2}\Big)\tilde{d}_L^2 + \sum_{k=v,L}\kappa_k\tilde{d}_k\dot{d}_k,\end{aligned} \tag{21}$$

The inequality (21) can be rearranged with the constants $\kappa := \frac{1}{\omega_{cc}}\Big(\frac{3}{4\omega_{vc}C_0^2} + 1\Big)$, $\kappa_v := \frac{1}{l_v}\Big(\frac{3}{4\omega_{vc}C_0^2} + \frac{1}{2}\Big)$, and $\kappa_L := \frac{1}{l_L}\Big(\frac{\kappa^2}{2L_0^2} + \frac{1}{2}\Big)$ as

$$\begin{aligned}\dot{V} &\le -\frac{\omega_{vc}}{3}\tilde{v}_{\mathrm{dc}}^2 - \frac{1}{2}\tilde{i}_L^2 - \rho_{\mathrm{at}}\tilde{\omega}_{vc}^2 - \sum_{k=v,L}\frac{1}{2}\tilde{d}_k^2 \\ &\quad + \sum_{k=v,L}\kappa_k\dot{d}_k\tilde{d}_k + \dot{v}_{\mathrm{dc,ref}}\tilde{v}_{\mathrm{dc}} \\ &\le -\alpha V + \boldsymbol{w}^{\mathrm{T}}\boldsymbol{y},\end{aligned} \tag{22}$$

where $\alpha := \min\Big\{\frac{2\omega_{vc}}{3}, \frac{1}{\kappa}, \gamma_{\mathrm{at}}\sigma_{\mathrm{at}}, \frac{1}{\kappa_v}, \frac{1}{\kappa_L}\Big\}$, $\boldsymbol{w} := \begin{bmatrix}\dot{v}_{\mathrm{dc,ref}} & \kappa_v\dot{d}_v & \kappa_L\dot{d}_L\end{bmatrix}$, and $\boldsymbol{y} := [\tilde{v}_{\mathrm{dc}} \quad \tilde{d}_v \quad \tilde{d}_L]$. This result indicates the $\mathscr{L}_2$-stability for the input–output mapping of $\boldsymbol{w} \mapsto \boldsymbol{y}$, and hence, the exponential convergence property of (18) holds as $\dot{v}_{\mathrm{dc,ref}}, \dot{d}_v, \dot{d}_L \to 0$ exponentially. □

Lemma 1 analyses the cut-off frequency behaviour obtained from the proposed auto-tuner (8), which is used to derive the performance recovery property in Theorem 2.

Lemma 1: The proposed auto-tuner (8) ensures that the cut-off frequency $\hat{\omega}_{vc}(t)$ is bounded below from its initial value of $\hat{\omega}_{vc}(0) = \omega_{vc}$, i.e.

$$\hat{\omega}_{vc}(t) \ge \omega_{vc}\,. \tag{23}$$

Proof: The proposed auto-tuner (8) can be rearranged as

$$\dot{\hat{\omega}}_{vc} = -\gamma_{\mathrm{at}}\rho_{\mathrm{at}}\hat{\omega}_{vc} + \gamma_{\mathrm{at}}\rho_{\mathrm{at}}\omega_{vc} + \gamma_{\mathrm{at}}\tilde{v}_{\mathrm{dc}}^2,$$

and integrating both sides yields

$$\begin{aligned}\hat{\omega}_{vc} &= \mathrm{e}^{-\gamma_{\mathrm{at}}\rho_{\mathrm{at}}t}\omega_{vc} \\ &\quad + \int_0^t e^{-\gamma_{\mathrm{at}}\rho_{\mathrm{at}}(t-\tau)}(\gamma_{\mathrm{at}}\rho_{\mathrm{at}}\omega_{vc} + \gamma_{\mathrm{at}}\tilde{v}_{\mathrm{dc}}^2)\mathrm{d}\tau \\ &\quad \ge \mathrm{e}^{-\gamma_{\mathrm{at}}\rho_{\mathrm{at}}t}\omega_{vc} + \gamma_{\mathrm{at}}\rho_{\mathrm{at}}\omega_{vc}\mathrm{e}^{-\gamma_{\mathrm{at}}\rho_{\mathrm{at}}t}\int_0^t \mathrm{e}^{\gamma_{\mathrm{at}}\rho_{\mathrm{at}}\tau}\mathrm{d}\tau \\ &= \omega_{vc},\end{aligned}$$

which confirms the result of Lemma 1. □

Theorem 2 asserts the performance recovery property of the closed-loop system using the result of Lemma 1.

Theorem 2: The closed-loop control scheme exponentially recovers the target tracking performance of (3), i.e.

$$\lim_{t\to\infty} v_{\mathrm{dc}}(t) = v_{\mathrm{dc}}^*(t) \tag{24}$$

as $\dot{d}_k(t)$ tends exponentially towards zero, $k = v, L$.

Proof: Combining (6) and (7) leads to the closed-loop output voltage dynamics as

$$\dot{v}_{\mathrm{dc}} = \hat{\omega}_{vc}(v_{\mathrm{dc,ref}} - v_{\mathrm{dc}}) - \frac{(1-u)}{C_0}\tilde{i}_L + \frac{1}{C_0}\tilde{d}_v\,. \tag{25}$$

By defining the error variable as $\tilde{v}_{\mathrm{dc}}^* := v_{\mathrm{dc}}^* - v_{\mathrm{dc}}$, (3) and (25) yield

$$\dot{\tilde{v}}_{\mathrm{dc}}^* = -\hat{\omega}_{vc}\tilde{v}_{\mathrm{dc}}^* + \frac{(1-u)}{C_0}\tilde{i}_L - \frac{1}{C_0}\tilde{d}_v\,. \tag{26}$$

Consider the positive definite function given by

$$V^* := \frac{1}{2}(\tilde{v}_{\mathrm{dc}}^*)^2 + \frac{c}{2}\tilde{i}_L^2 + \sum_{k=v,L}\frac{c_k}{2}\tilde{d}_k^2, \quad c > 0, c_k > 0,$$

whose time derivative along the trajectories (17), (19), and (26) is described as

$$\begin{aligned}\dot{V}^* &= \tilde{v}_{\rm dc}^*\dot{\tilde{v}}_{\rm dc}^* + c\tilde{i}_L\dot{\tilde{i}}_L + c_v\tilde{d}_v\dot{\tilde{d}}_v + c_L\tilde{d}_L\dot{\tilde{d}}_L \\ &\le -\hat{\omega}_{vc}(\tilde{v}_{\rm dc}^*)^2 + \tilde{v}_{\rm dc}^*\frac{(1-u)}{C_0}\tilde{i}_L - \frac{1}{C_0}\tilde{v}_{\rm dc}^*\tilde{d}_v \\ &\quad -c\omega_{cc}\tilde{i}_L^2 + \frac{c}{L_0}\tilde{i}_L\tilde{d}_L - c_v l_v\tilde{d}_v^2 + c_v\dot{d}_v\tilde{d}_v \\ &\quad -c_L l_L\tilde{d}_L^2 + c_L\dot{d}_L\tilde{d}_L\,.\end{aligned}$$

An upper bound of $\dot{V}^*$ can be obtained using the Young's inequality and the result of Lemma 1 as

$$\begin{aligned}\dot{V}^* \le &-\frac{\omega_{vc}}{3}(\tilde{v}_{\rm dc}^*)^2 - \left(c\omega_{cc} - \frac{3}{4\omega_{vc}C_0^2} - \frac{1}{2}\right)\tilde{i}_L^2 \\ &-\left(c_v l_v - \frac{3}{4\omega_{vc}C_0^2}\right)\tilde{d}_v^2 - \left(c_L l_L - \frac{c^2}{2L_0^2}\right)\tilde{d}_L^2 \\ &+\sum_{k=v,L} c_k\dot{d}_k\tilde{d}_k\,.\end{aligned} \tag{27}$$

The inequality (22) can be rearranged with the constants $c := \frac{1}{\omega_{cc}}\left(\frac{3}{4\omega_{vc}C_0^2}+1\right)$, $c_v := \frac{1}{l_v}\left(\frac{3}{4\omega_{vc}C_0^2}+\frac{1}{2}\right)$, $c_L := \frac{1}{l_L}\left(\frac{c^2}{2L_0^2}+\frac{1}{2}\right)$, and $\gamma^* := \min\left\{\frac{2\omega_{vc}}{3}, \frac{1}{c}, \frac{1}{c_v}, \frac{1}{c_L}\right\}$ as

$$\begin{aligned}\dot{V}^* &\le -\frac{\omega_{vc}}{3}(\tilde{v}_{\rm dc}^*)^2 - \frac{1}{2}\tilde{i}_L^2 - \sum_{k=v,L}\frac{1}{2}\tilde{d}_k^2 + \sum_{k=v,L} c_k\dot{d}_k\tilde{d}_k \\ &\le -\gamma^* V^* + \sum_{k=v,L} c_k\dot{d}_k\tilde{d}_k,\end{aligned}$$

which indicates the performance recovery property of (24) as $\dot{d}_v$ and $\dot{d}_L$ tend exponentially towards zero. □

The proposed control law of (14) and (7) does not incorporate the integration actions of the tracking errors. In actual implementations, the closed-loop system might suffer from steady-state errors. This issue is rigorously addressed by Theorem 3.

Theorem 3: The proposed controller comprising (7)–(10) and (14)–(16) ensures that

$$v_{\rm dc}(\infty) = v_{\rm dc,ref}(\infty), \tag{28}$$

where $\lim_{t\to\infty} v_{\rm dc}(t) = v_{\rm dc}(\infty)$ and $\lim_{t\to\infty} v_{\rm dc,ref}(t) = v_{\rm dc,ref}(\infty)$.

Proof: The error dynamics of (11), (17), and (19) yields the steady-state equations

$$\begin{aligned}0 = &-\hat{\omega}_{vc}(\infty)\tilde{v}_{\rm dc}(\infty) + \frac{(1-u(\infty))}{C_0}\tilde{i}_L(\infty) \\ &-\frac{1}{C_0}\tilde{d}_v(\infty),\end{aligned} \tag{29}$$

$$0 = -\omega_{cc}\tilde{i}_L(\infty) + \frac{1}{L_0}\tilde{d}_L(\infty), \tag{30}$$

$$0 = -l_k\tilde{d}_k(\infty), \quad k = v, L, \tag{31}$$

where $\lim_{t\to\infty} f(t) = f(\infty)$ for any scalar function $f(\cdot)$. By combining (29), (30), and (31), $\tilde{v}_{\rm dc}(\infty) = 0$ is derived. Therefore, the assertion in Theorem 3 holds true. □

Remark 1: This remark provides a systematic tuning guideline for the proposed controller.

(i) Set the design parameters for the DOBs and auto-tuner as $l_v = l_L = 0$ and $\gamma_{st} = \rho_{st} = 0$, respectively.
(ii) Increase the cut-off frequency w_{vc} from a small positive value until an appropriate transient performance is obtained, whereas the cut-off frequency w_{cc} is always set to be at least ten times w_{vc} to separate the dynamics of the inner and outer loops.
(iii) Increase the DOB design parameters l_v and l_L from small positive values to some values at which the steady-state errors disappear with no noise amplification.
(iv) Increase the auto-tuner design parameter γ_{st} from a small positive value until a satisfying transient performance is obtained with the design parameter $\rho_{st} = \frac{1}{\tau\gamma_{st}}$, where τ is the time constant for the control gain to return to its initial value. It is recommended to set τ to ∼5.

4 Experimental results

4.1 Experimental setup

Experimental verification was conducted using a 5 kW prototype DC/DC boost converter to verify the effectiveness of the proposed controller whose schematic is shown in Fig. 2. A DSP28377 (Texas Instruments) was used to implement the proposed controller with control and pulse-width modulation periods of 0.1 ms. The inductor and capacitor values for the converter were given as $L = 1$ mH and $C = 700\,\mu$F, respectively, and their nominal values were assumed to be $L_0 = 0.7$ LmH and $C_0 = 1.2$ CμF, respectively, to consider model-plant mismatches. The input DC source voltage was initially set to $v_{\rm in,0} = 50$ V. Fig. 3 shows the experimental setup. The output voltage tracking and regulation performance of the proposed controller were evaluated under linear and non-linear load conditions in comparison with those of the conventional FL controller. The effects of the auto-tuner design parameter on the tracking performance were also investigated. The gain selection of the proposed and FL controllers is presented in the following subsection.

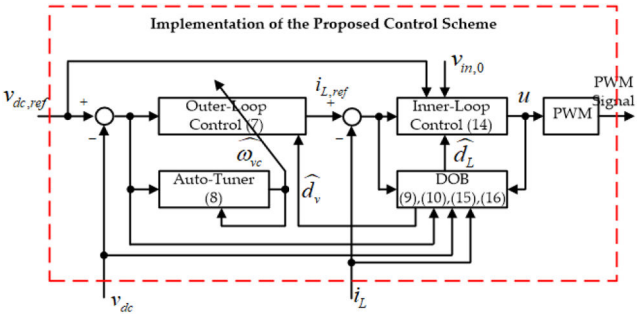

Fig. 2 *Schematic of the control algorithm*

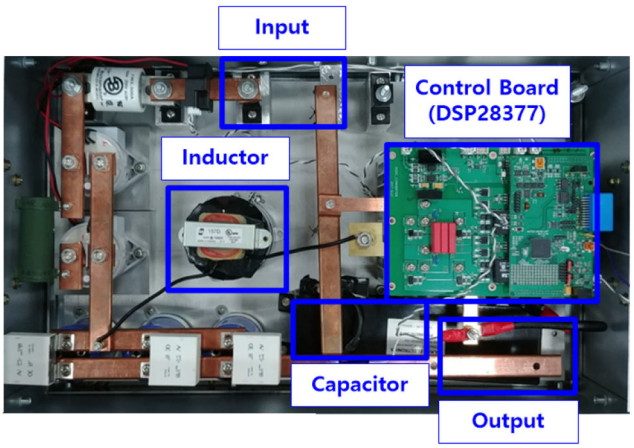

Fig. 3 *Experimental setup*

IET Power Electron., 2019, Vol. 12 Iss. 14, pp. 3767-3773

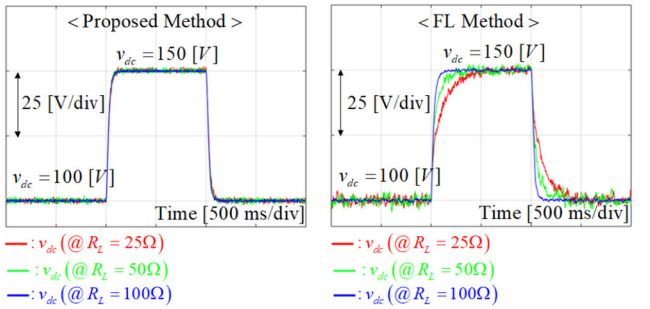

Fig. 4 *Output voltage tracking responses under the three resistive loads of* $R_L = 25, 50, 100\,\Omega$

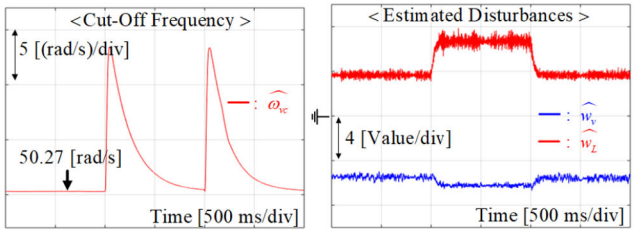

Fig. 5 *Cut-off frequency and estimated disturbance behaviours under the resistive load of* $R_L = 25\,\Omega$

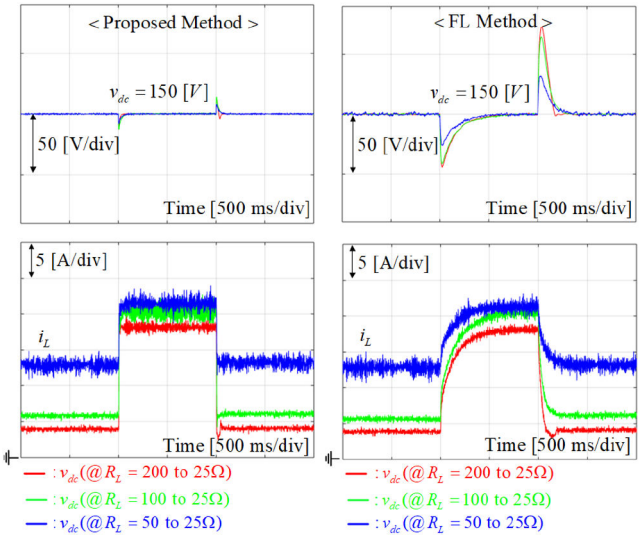

Fig. 6 *Output voltage regulation responses under the three load changes between* $R_L = 50, 100, 200\,\Omega$ *and* $R_L = 25\,\Omega$ *in a stepwise manner*

4.2 Controller gain selection

The gains of the proposed controller were set to be $\omega_{vc} = 50.27$, $\omega_{cc} = 628.3$, $l_v = l_L = 314.2$, $\gamma_{st} = 0.8$, and $\rho_{st} = 6.25$ based on the guideline presented in Remark 1.

The FL controller is given by

$$u(t) = \frac{1}{v_{\rm dc}(t)}\left(K_{pc}\tilde{i}_L(t) + K_{ic}\int_0^t \tilde{i}_L(\tau)\mathrm{d}\tau + (v_{\rm dc}(t) - v_{\rm in})\right), \tag{32}$$

$$i_{L,ref}(t) = K_{pv}\tilde{v}_{dc}(t) + K_{iv}\int_0^t \tilde{v}_{dc}(\tau)\mathrm{d}\tau\,. \tag{33}$$

By selecting the control gains using the nominal parameters L_0 and C_0, and the cut-off frequencies w_{vc} and w_{cc} as

$$K_{pc} = 2L_0\omega_{cc}, K_{ic} = L_0\omega_{cc}^2,$$

$$K_{pv} = \frac{1}{1-u(t)}2C_0\omega_{vc}, K_{iv} = \frac{1}{1-u(t)}C_0\omega_{vc}^2$$

the following frequency responses are obtained:

$$V_{\rm dc}(s) = \frac{\omega_{vc}}{s+\omega_{vc}}V_{\rm dc,ref}(s) + \frac{\omega_{vc}s}{(s+\omega_{vc})^2}V_{\rm dc,ref}(s) + \frac{s}{C_0(s+\omega_{vc})^2}D_{v,0}(s) \tag{34}$$

$$I_L(s) = \frac{\omega_{cc}}{s+\omega_{cc}}I_{L,\rm ref}(s) + \frac{\omega_{cc}s}{(s+\omega_{cc})^2}I_{L,\rm ref}(s) + \frac{s}{L_0(s+\omega_{cc})^2}D_{L,0}(s),\ \forall s \in \mathbb{C}, \tag{35}$$

where $D_{v,0}(s)$ is the Laplace transform of $d_{v,0}(t) := d_v(t) - (1-u(t))\tilde{i}_L(t)$. As the second and third terms on the right-hand sides of (34) and (35), which represent the second-order dynamics caused by the integrators and disturbances, respectively, are negligible for sufficiently small s, they can be approximated by the following closed-loop transfer functions:

$$\frac{V_{\rm dc}(s)}{V_{\rm dc,ref}(s)} \simeq \frac{\omega_{vc}}{s+\omega_{vc}}, \frac{I_L(s)}{I_{L,\rm ref}(s)} \simeq \frac{\omega_{cc}}{s+\omega_{cc}}.$$

The cut-off frequencies of the FL controller were set to be equal to those of the proposed controller for fairness of comparison. The experimental results under linear and non-linear load conditions are provided in Sections 4.3 and 4.4, respectively.

Remark 2: The second and third terms on the right-hand sides of (34) and (35) cannot be ignored in transient conditions with non-negligible s. The adverse effects from these terms are only suppressed indirectly by a cut-off frequency tuning, for which it is difficult to formulate a systematic guideline. By contrast, the proposed controller includes the auto-tuner and DOBs to suppress directly the effects from disturbances, and the controller gains can be easily selected based on the guideline presented in Remark 1.

4.3 Experiments under linear load conditions

4.3.1 Evaluation of tracking performance: The reference output voltage $v_{\rm dc,ref}(t)$ increased from 100 to 150 V at $t = 1$ s and decreased back to 100 V at $t = 2$ s under three resistive load conditions $R_L = 25$, 50, 100 Ω. Fig. 4 shows the resulting output voltage responses, which demonstrate that the proposed controller provided uniform output voltage responses for the three different load conditions, even with the fixed design parameters. By contrast, the FL controller showed different transient performances depending on the load conditions. The time-varying cut-off frequency adjusted by the auto-tuner and the estimated disturbance from the DOBs under the resistive load condition of $R_L = 25\,\Omega$ are presented in Fig. 5.

4.3.2 Evaluation of regulation performance: The reference output voltage was given by $v_{\rm dc,ref}(t) = 150$ V with sudden load changes where the resistive load was changed from $R_L = 50, 100$ and $200\,\Omega$ to $R_L = 25\,\Omega$ at $t = 1$ s, and returned to its initial value at $t = 2$ s. The resulting output voltage responses for the three load changes are shown in Fig. 6, which verifies the effectiveness of the proposed method with the remarkable reductions in the under- and over-shoot while rapidly driving the inductor current.

4.3.3 Effect of auto-tuner design parameter on tracking performance: The effect of the auto-tuner design parameter on the tracking performance was investigated in an identical scenario to the experiment in Section 4.3.1 with a resistive load of $R_L = 25\,\Omega$. The design parameter ρ_{st} was changed from 0 (i.e. the auto-tuner is

disabled) to 0.4 and 3, whereas the design parameter γ_{st} was maintained the same as that in the previous experiments. The initial cut-off frequency w_{vc} was set to 1 Hz to observe the effect of the auto-tuner. The resultant output voltage responses and the corresponding behaviours of the cut-off frequency are presented in Fig. 7. As expected, the output voltage tracking performance was enhanced by the auto-tuner, which automatically adjusted the cut-off frequency. Notably, this transient performance improvement did not yield an increase in the sensitivity of the control system, which can be indirectly judged by the noise level of the output voltage. The trade-off between the transient performance and sensitivity can be resolved by increasing the cut-off frequency only in transient states.

4.4 Experiments under non-linear load conditions

A 3 kW permanent magnet synchronous motor (PMSM) driven by a voltage–source inverter (VSI) was used to provide non-linear load conditions. The specifications of the PMSM drive are listed in Table 1. The non-linear load conditions were changed by the stator current (I_s) of the PMSM, whereas the rotational speed of the PMSM was controlled to be constant at 1000 RPM using a load motor.

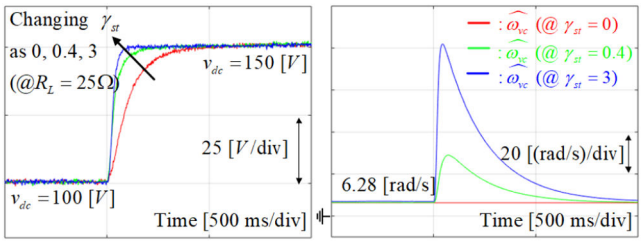

Fig. 7 *Output voltage tracking responses and the corresponding cut-off frequency behaviours for the three different auto-tuner design parameters* $\rho_{st} = 0,\ 0.4,\ 3$

Table 1 PMSM drive specifications

DC-link voltage	100 V
rated stator current	50 A
rated speed	1200 rpm
rated torque	40 Nm
switching frequency	10 kHz

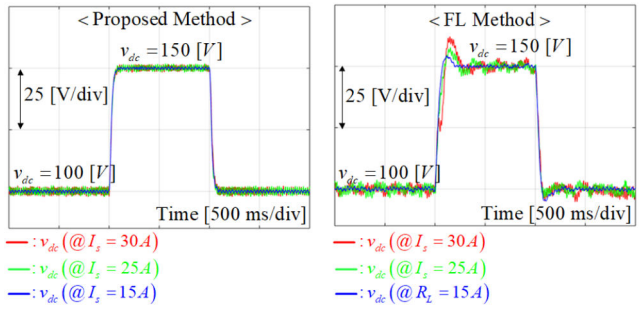

Fig. 8 *Output voltage tracking responses under the three non-linear loads of* $I_s = 15, 25, 30$ A

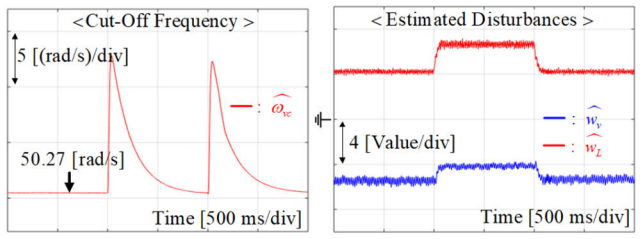

Fig. 9 *Cut-off frequency and estimated disturbance behaviours under the non-linear load of* $I_s = 30$ A

4.4.1 Evaluation of tracking performance: The reference output voltage $v_{dc,ref}(t)$ increased from 100 to 150 V at $t = 1$ s and decreased back to 100 V at $t = 2$ s under three load conditions $I_s = 15, 25, 30$ A. Fig. 8 shows the resulting output voltage responses, which demonstrate that the proposed controller also provided uniform output voltage responses for the non-linear loads, even with the fixed design parameters. By contrast, the FL controller yielded over-shoots that varied with the load. The time-varying cut-off frequency adjusted by the auto-tuner and the estimated disturbance from the DOBs under the load conditions of $I_s = 30$ A are shown in Fig. 9.

4.4.2 Evaluation of regulation performance: The reference output voltage was given by $v_{dc,ref}(t) = 150$ V with sudden load changes where the stator current was changed from $I_s = 30$ A to $I_s = 5, 10$ and 20 A at $t = 1$ s, and returned to its initial value at $t = 2$ s. The resulting output voltage responses for the three load changes are shown in Fig. 10, which also verifies the effectiveness of the proposed method for non-linear loads with the remarkable reductions in the under- and over-shoot while rapidly driving the inductor current. However, the inductor current obtained with the proposed method showed higher ripple than that obtained with the FL method. This is because the proposed method, which was shown to have a higher cut-off frequency than the FL method, responded sensitively to the switching harmonics caused by the VSI load. Increasing the cut-off frequency of the control system inevitably increases the sensitivity to high-frequency components. Nonetheless, the inductor current ripple of the proposed method can be significantly reduced if the switching operations of the VSI and converter can be synchronised so that no switching harmonics are measured at the control step of the converter.

4.4.3 Effect of auto-tuner design parameter on tracking performance: The effect of the auto-tuner design parameter on the tracking performance was investigated in an identical scenario to the experiment in Section 4.4.1 with a non-linear load of $I_s = 30$ A. The design parameter ρ_{st} was changed from 0 (i.e. the auto-tuner is disabled) to 0.4 and 3 while the design parameter γ_{st} was maintained the same as that in the previous experiments. The initial cut-off frequency w_{vc} was set to 1 Hz to observe the effect of the auto-tuner. The resultant output voltage responses and the corresponding behaviours of the cut-off frequency are presented in Fig. 11. As expected, the output voltage tracking performance was enhanced by the auto-tuner, which automatically adjusted the cut-off frequency.

The experimental results confirmed that the proposed method provided enhanced and uniform transient performance for the output voltage control regardless of the type and degree of load even in the presence of model-plant mismatches without any steady-state errors. The performance of the conventional FL controller could also be improved by scheduling control gains depending on the operating conditions. However, the gain scheduling approach requires expensive experimental efforts to tune the control gains manually or heavy computational burden to solve the optimisation problems under various constraints in real time [9]. By contrast, the proposed controller consists of several predetermined equations including the outer- and inner-loop control laws, auto-tuner, and DOBs, which are relatively easy to implement compared with the FL controller with gain scheduling. These properties would be highly beneficial for electric vehicle and solar power generation applications where the parameter and load variations are large. The proposed control technique could be a reasonable alternative to the conventional methods.

5 Conclusions

In this study, a non-linear output voltage tracking controller for DC/DC boost converters was proposed. An auto-tuning algorithm, which automatically updates the control gain during transient periods, was devised as a means of improving the transient performance. A proportional-type control law and DOBs were

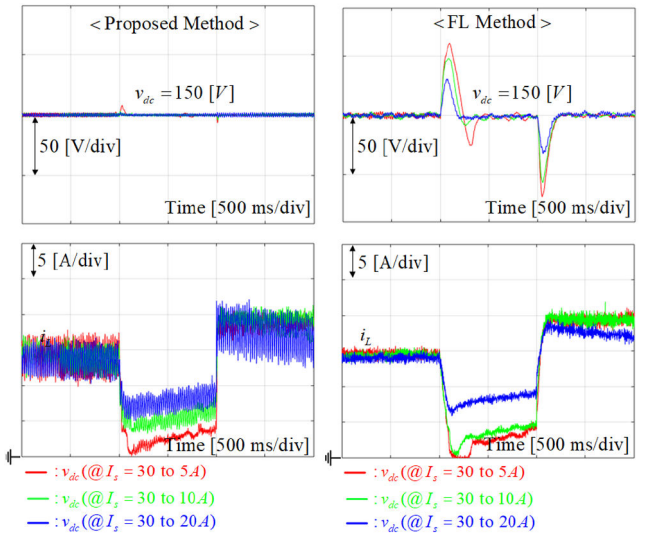

Fig. 10 *Output voltage regulation responses under the three load changes between* $I_s = 30$ A *and* $I_s = 5, 10, 20$ A *in a stepwise manner*

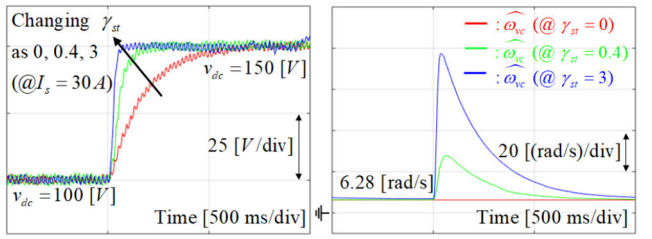

Fig. 11 *Output voltage tracking responses and the corresponding cut-off frequency behaviours for the three different auto-tuner design parameters of* $\rho_{st} = 0, 0.4, 3$

designed for the output voltage control together with the auto-tuner. Theoretical and experimental analyses showed that the closed-loop system provided enhanced and uniform transient performance even in the presence of system uncertainties without any steady-state errors.

6 Acknowledgments

This research was supported by a grant (17TLRP-C135446-01, Development of Hybrid Electric Vehicle Conversion Kit for Diesel Delivery Trucks and its Commercialisation for Parcel Services) from the Transportation & Logistics Research Program (TLRP) funded by the Ministry of Land, Infrastructure and Transport of Korean Government.

7 References

[1] Adam, G.P., Abdelsalam, I., Xu, L., *et al.*: 'Multi-tasking dc–dc and dc–ac converters for dc voltage tapping and power control in highly meshed multi-terminal HVDC networks', *IET Power Electron.*, 2017, **10**, pp. 2217–2228

[2] Wang, Y., Wang, F., Lin, Y., *et al.*: 'Sensorless parameter estimation and current-sharing strategy in two-phase and multiphase IPOP DAB DC–DC converters', *IET Power Electron.*, 2018, **11**, pp. 1135–1142

[3] Aboushady, A.A., Ahmed, K.H., Finney, S.J., *et al.*: 'Lyapunov-based high-performance controller for modular resonant DC/DC converters for medium-voltage DC grids', *IET Power Electron.*, 2017, **10**, pp. 2055–2064

[4] Sun, C., Zhang, J., Cai, X., *et al.*: 'Voltage balancing control of isolated modular multilevel dc–dc converter for use in dc grids with zero voltage switching', *IET Power Electron.*, 2016, **9**, pp. 270–280

[5] Adam, G.P., Gowaid, I.A., Finney, S.J., *et al.*: 'Review of dc–dc converters for multi-terminal HVDC transmission networks', *IET Power Electron.*, 2016, **9**, pp. 281–296

[6] Gavagsaz-Ghoachani, R., Saublet, L.-M., Phattanasak, M., *et al.*: 'Active stabilisation design of DC–DC converters with constant power load using a sampled discrete-time model: stability analysis and experimental verification', *IET Power Electron.*, 2018, **11**, pp. 1519–1528

[7] Erickson, R.W., Maksimovic, D.: '*Fundamentals of power electronics*' (Springer-Verlag, New York, 2001, 2nd edn.)

[8] Alexander, G.P., Feng, G., Yan-Fei, L., *et al.*: 'A design method for PI-like fuzzy logic controllers for DC/DC converter', *IEEE Trans. Ind. Electron.*, 2007, **54**, pp. 2688–2696

[9] Olalla, C., Leyva, R., Queinnec, I., *et al.*: 'Robust gain-scheduled control of switched-mode DC–DC converters', *IEEE Trans. Power Electron.*, 2012, **27**, pp. 3006–3019

[10] Su, J.-T., Liu, C.-W.: 'Gain scheduling control scheme for improved transient response of DC–DC converters', *IET Power Electron.*, 2012, **5**, pp. 678–692

[11] Oucheriah, S., Guo, L.: 'PWM-based adaptive sliding-mode control for boost DC/DC converters', *IEEE Trans. Ind. Electron.*, 2013, **60**, pp. 3291–3294

[12] Flores, J.L., Mendez, A.H., Rodriguez, C.G., *et al.*: 'Robust nonlinear adaptive control of a boost converter via algebraic parameter identification', *IEEE Trans. Ind. Electron.*, 2014, **61**, pp. 4105–4114

[13] Xiong Wang, Y., Hyun Yu, D., Bae Kim, Y.: 'Robust time-delay control for the DC/DC boost converter', *IEEE Trans. Ind. Electron.*, 2014, **61**, pp. 4829–4837

[14] Salimi, M.: 'Sliding mode control of the DC–DC fly back converter with zero steady-state error', *J. Basic Appl. Sci. Res.*, 2012, **2**, pp. 10693–10705

[15] Wai, R.-J., Shih, L.-C.: 'Design of voltage tracking control for DC–DC boost converter via total sliding-mode technique', *IEEE Trans. Ind. Electron.*, 2011, **58**, pp. 2502–2511

[16] Zhang, Q., Min, R., Tong, Q., *et al.*: 'Sensorless predictive current controlled DC–DC converter with a self-correction differential current observer', *IEEE Trans. Ind. Electron.*, 2014, **61**, pp. 6747–6757

[17] Kim, S.-K., Park, C.R., Lee, Y.I.: 'A stabilizing model predictive controller for voltage regulation of a DC/DC boost converter', *IEEE Trans. Control Syst. Technol.*, 2014, **41**, pp. 2107–2114

[18] Kim, S.-K., Kim, J.-S., Park, C.R., *et al.*: 'Output-feedback model predictive controller for voltage regulation of a DC/DC converter', *IET Control Theory Appl.*, 2013, **7**, pp. 1959–1968

[19] Beccuti, A.G., Mariethoz, S., Cliquennois, S., *et al.*: 'Explicit model predictive control of DC/DC switched-mode power supplies with extended kalman filtering', *IEEE Trans. Ind. Electron.*, 2009, **56**, pp. 1864–1874

[20] Karamanakos, P., Geyer, T., Manias, S.: 'Direct voltage control of DC–DC boost converters using enumeration-based model predictive control', *IEEE Trans. Power Electron.*, 2014, **29**, pp. 968–978

[21] Bibian, S., Jin, H.: 'High performance predictive dead-beat digital controller for DC power supplies', *IEEE Trans. Power Electron.*, 2002, **17**, pp. 420–427